Fractal Analysis of Medical Images in the Irregular Regions of Interest

Edward Oczeretko, Marta Borowska, Agnieszka Kitlas, Andrzej Borusiewicz,
and Malgorzata Sobolewska-Siemieniuk

***Abstract*— For medical images diagnostically important information often lies in the texture. Fractal dimension may be used as an index of irregularity. In this paper we describe the adaptation of the intensity difference scaling method for assessment of the fractal dimension D in the irregular regions of interest (irregular ROI-s). This is of great importance because the investigated regions are often small. It is difficult to fit entire regular region of interest within the examined organ with simultaneous inclusion of the relevant fragment, and at the same time to avoid the influence of boundaries. Fractal analysis of various kinds of medical images: panoramic radiography and nuclear medicine scan showed the validity of assessment of D in irregular ROI-s.**

I. INTRODUCTION

FRACTAL analysis has been successfully applied in many areas of science and technology. Applications in medicine concern modelling of tissues and organs constitution and analyzing of different kinds of images and time series [1]. The fractal objects are characterized by [2]: large degree of heterogeneity, self-similarity, and lack of a well-defined scale. Notion „self-similarity" means that small-scale structures of fractal set resemble large-scale structures.

The fractional Brownian motion (fBm) following the Mandelbrot's fractal theory, may be used to describe the roughness of natural surfaces. It regards naturally occurring surfaces as the end result of random walks [3]. Medical images can be treated as surfaces with the intensity at each point (x,y). For nuclear medicine images, the intensity I is a number of counts of gamma radiation quantum, whereas for radiological or ultrasonic images the intensity is estimated by the grey levels. For different surfaces the values of the fractal dimension are in the range between 2 and 3. A smooth surface is characterized by fractal dimension of about 2; rougher surfaces have higher fractal dimensions. The fractal dimension may be used as an index of heterogeneity. In the language of mathematics, fractals are the sets for which the Hausdorff-Besicovitch dimension, or the fractal dimension D are greater than topological dimension. The fractal dimension may be calculated in many ways since Hausdorff-Besicovitch's definition is too complicated for practical estimation [4], [5]. However, it has helped to create many other definitions and subsequent algorithms. Hausdorff definition is a mathematical foundation of various methods of the fractal dimension estimating. Thus, according to various algorithms, there are various kinds of fractal dimension.

For all methods, there is relation between fractal dimension and various kinds of scales: length, area size, volume, intensity, frequency. The relationship between selected parameters is governed by a power-law

$$M(\delta) = const \cdot \delta^{exponent} \tag{1}$$

where $M(\delta)$ is a measure, δ is a scale, *exponent* is directly related with the value of fractal dimension

Among the algorithms are: rectangular prism surface area method [6]; triangular prism surface area method [7]; power spectral density method [8], [9]; methods based on mathematical morphology: flat structuring element method [10] and cover blanket method [11]; dispersion analysis [12], [13]; variogram analysis [14]; intensity difference scaling method [15]; box dimension [16], [17].

These methods were applied in the analysis of various kinds of medical images [18], [19], [20], [21], [22], [23]. In all the cases the studies were performed in regular regions of interest (regular ROI-s) — mostly square regions. In the literature calculation of fractal dimension in irregular regions of interest was mentioned only once but without the description of the algorithm [13]. Oczeretko et al. showed that in the case of the lung scintigrams, $D = 2.23$ in the region containing the boundary of the organ and $D = 2.59$ within the organ. Great local irregularities and sharp edges of the examined objects accounted for estimated values of fractal dimension $D \approx 2$ [24]. In order to avoid the influence of the boundaries, and other structures it would be proper to calculate the fractal dimensions in irregular ROI-s.

In this paper we describe the adaptation of the intensity difference scaling method for the assessment of the fractal dimension in the irregular regions of interest.

II. INTENSITY DIFFERENCE SCALING METHOD

Intensity difference scaling method was introduced by Chen et al. [15]. The texture of the intensity image $I(\vec{r})$ can be modeled by a fractional Brownian function [2]:

$$Pr\left(\frac{I(\vec{r}+\Delta\vec{r}) - I(\vec{r})}{|\Delta\vec{r}|^H} < y\right) = F(y) \tag{2}$$

Manuscript received June 10, 2008.

E. Oczeretko is with the Department of Medical Informatics, University of Bialystok, Bialystok, and with Faculty of Informatics, Academy of Agrobusiness, Lomza, Poland (phone: ++48-85-7457662; fax: ++48-85-7457662; e-mail: eddoczer@ii.uwb.edu.pl)

M. Borowska is with Department of Medical Informatics, University of Bialystok, Bialystok, Poland (e-mail: mborowska@ii.uwb.edu.pl)

A. Kitlas is with Department of Medical Informatics, University of Bialystok, Bialystok, Poland (e-mail: akitlas@ii.uwb.edu.pl)

A Borusiewicz is with Faculty of Informatics, Academy of Agrobusiness, Lomza, Poland (e-mail: andrzej.borusiewicz@wsa.edu.pl)

M. Sobolewska-Siemieniuk is with Department of Orthodontics, Medical University of Bialystok, Bialystok, Poland (e-mail: sobolewska.m@op.pl)

where $\vec{r} = (x,y)$ — the position in two dimensional space, $I(\vec{r})$ — the intensity of pixel at position $\vec{r}$, $F(y)$ — the cumulative distribution function, H — Hurst coefficient. H is the constant and lies in the range $0 < H < 1$. The relationship between the fractal dimension D the Hurst coefficient H is $D = 3 - H$. From (2) we can derive [24]:

$$E\{[I(\vec{r}+\Delta\vec{r}) - I(\vec{r})]^2\} = |\Delta\vec{r}|^{2H} \cdot \sigma^2 \tag{3}$$

where E is the expectation, σ^2 is the variance of the $F(y)$. Defining:

$$\Delta I_{\vec{r}} = |I(\vec{r}+\Delta\vec{r}) - I(\vec{r})| \tag{4}$$

and taking the logarithm of (3), we can obtain:

$$\log E\{\Delta I_{\vec{r}}^2\} = 2H \log|\Delta\vec{r}| + 2\log\sigma^2 = 2H\log|\Delta\vec{r}| + \log C \tag{5}$$

Since both H and C are constants, (5) implies that a plot of $E\{\Delta I_{\vec{r}}^2\}$ as a function of $|\Delta\vec{r}|$ on the log-log scale lies on the straight line and its slope is H. This plot is called fractal plot. Equation (5) was simplified by Chen et al. to [15]:

$$\log E\{\Delta I_{\vec{r}}\} = H \log|\Delta\vec{r}| + \log C \tag{6}$$

Some authors have doubt about such a simplification, but the others bring out the validity of this algorithm in classification of ultrasonic and CT liver images [25], [26], [27].

In realization of this algorithm for given $M \times M$ image, the average of the absolute intensity difference $id(s)$ of all pixel pairs with scale s was defined as follows:

$$id(s) = \frac{\sum_{x1=0}^{M-1}\sum_{y1=0}^{M-1}\sum_{x2=0}^{M-1}\sum_{y2=0}^{M-1}(|\, I(x2,y2) - I(x1,y1)\,|)}{\text{number of pixel pairs for scale } s} \tag{7}$$

where: $I(x1,y1)$ and $I(x2,y2)$ are two pixels in the image with intensity values between 0 and 255; $x1$, $y1$, $x2$, $y2 = 1,2,3,\ldots,M-1$;

s – scale (distance between two pixels):

$$s = \sqrt{(x2-x1)^2 + (y2-y1)^2} \tag{8}$$

The multiscale intensity difference vector *MIDV* was introduced:

$$MIDV = [id(1), id(2), id(3), \ldots, id(s)] \tag{9}$$

Fig. 1 shows 3×3 image. There are 5 possible scales, 5 possible distances between pixels. The total number of pixel pairs analyzed for these scales is 36. For 27×27 images the number of all scales is 314, for 63×63 images the number of all scales is 1529, and the total number of pixel pairs analyzed for these scales is 31505922.

To reduce the number of elements of *MIDV* vector, normalized *NMIDV* vector was used in which only integer scales occurred. Non-integer scales were not lost. For example, information from scales: $\sqrt{5}$, $\sqrt{8}$ (2.2361, 2.8284) was included in scale 2. For fractal surfaces the relationship between *MIDV* and scale s is governed by a power-law:

$$MIDV = Cs^H \tag{10}$$

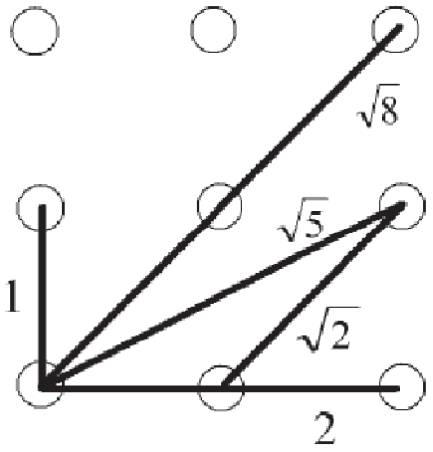

Fig. 1. 3×3 image. There are 5 possible scales. The total number of analyzed pixel pairs for these scales is 36.

Value of H was assessed by using least-squares linear regression to estimate the slope of line of *MIDV*, versus s in log-log scale. Fractal dimension was obtained as:

$$D = 3 - H \tag{11}$$

III. IRREGULAR REGIONS OF INTEREST

By means of the intensity difference scaling method we could assess the values of fractal dimension in irregular ROI-s, which is impossible by means of other algorithms.

Figure 2(a) shows the 5×5 image with 25 pixels and 14 possible scales: 1, $\sqrt{2}$, 2, $\sqrt{5}$, $\sqrt{8}$, 3, $\sqrt{10}$, $\sqrt{13}$, 4, $\sqrt{17}$, $\sqrt{18}$, $\sqrt{20}$, 5, $\sqrt{32}$. The total number of pixel pairs analyzed for these scales is 300. Fig 2(b) illustrates manually drawn irregular region of interest R with 12 pixels and 9 possible scales. In calculation only pixels belonging to regions R were used.

In practical realization of this algorithm (Fig. 3) the irregular regions of interest were drawn manually using a **roipoly** Matlab function (Matlab v. 5.2 for Windows (MathWorks, Inc., USA). This function is a part of the Image Processing Toolbox and returns a binary image, a binary mask M. The mask contains 1's for all pixels that are part of the ROI and 0's everywhere else. In order to perform a fractal analysis in the irregular regions of interest only pixels which coordinates belong to mask M were taken into account.

$$(x1,y1),(x2,y2) \in M$$

Fig. 3(a) shows the 63-by-63 image with irregular ROI. The obtained mask was shown in Fig. 3(b). The algorithm of assessing of fractal dimension was implemented in C++. The synthetic surface which is shown in Fig. 3, was generated for $D = 2.60$, estimated fractal dimension of such image is 2.585, estimated fractal dimension in irregular region of interest is 2.591.

IV. EXPERIMENTS

A. Synthetic Fractal Textures

Spatially isotropic synthetic surfaces (fBm images) which ranged in fractal dimension from 2.05 to 2.95 (2.05, 2.10,

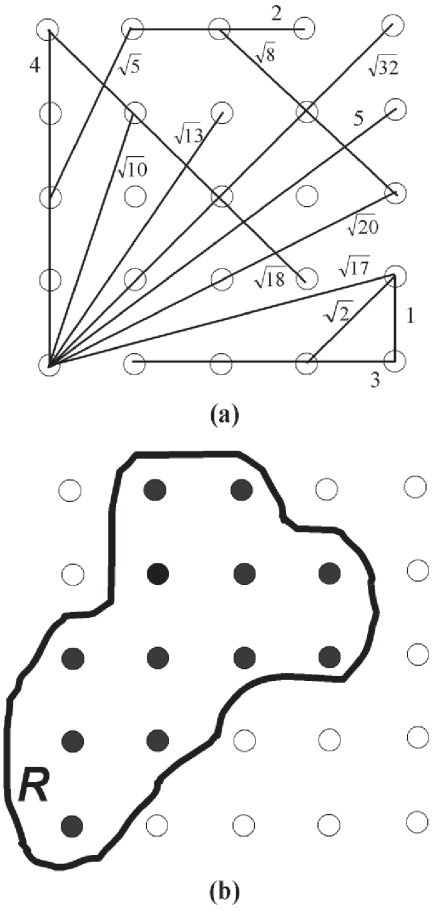

Fig. 2. (a) 5×5 image. There are 14 possible scales. The total number of pixel pairs analyzed for these scales is 300. (b) Manually drawn irregular region of interest R with 12 pixels and 9 possible scales.

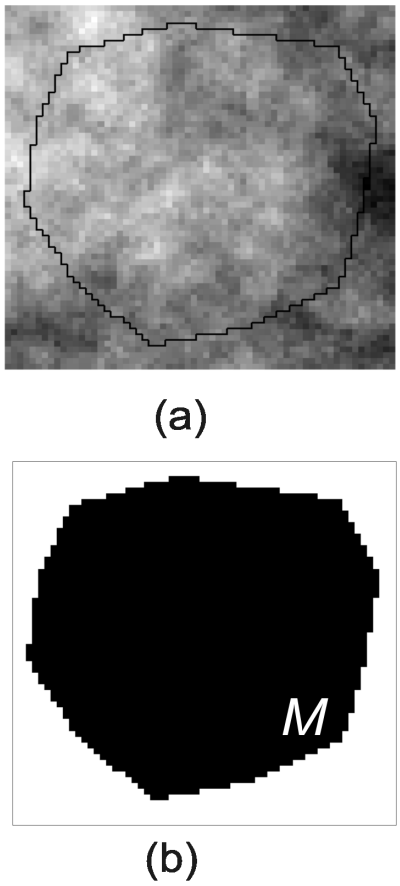

Fig. 3. Synthetic image of fractal dimension $D = 2.60$ with manually drawn irregular region of interest, b) binary image — mask M.

2.20, 2.30, 2.40, 2.50, 2.60, 2.70, 2.80, 2.90, 2.95) were generated by means of Matlab function **synth2**, that is a part of FracLab, a Fractal Analysis Software (www.scilab.org, e-mail: FracLab@inria.fr). Here incremental Fourier synthesis method was implemented to generate 2-D self similar images [28]. Fig. 4 shows an example of such surfaces with fractal dimensions equaling 2.20 and 2.80. For each value of fractal dimension thirty 63-by-63 images were obtained. The results of fractal analysis of such images by means of the intensity difference scaling method are tabulated in Table I. For each synthetic surface, an irregular region of interest which is shown in Fig. 3 was chosen. Table II shows the results of fractal analysis in irregular regions of interest drawn on synthetic textures. For each original dimension, the fractal dimension D and standard deviation σ were obtained in 30 realizations. Mean squared error (MSE) for the 330 samples for each table is calculated from the formula [29], [30]:

$$MSE = \sum_{i=1}^{11} [(meanD - D_j)^2 + \sigma_j^2] \qquad (12)$$

where the subscript j indicates a series of 30 runs. Mean squared errors for data represented in Tables I and II equal 0.0020, and 0.0017 respectively.

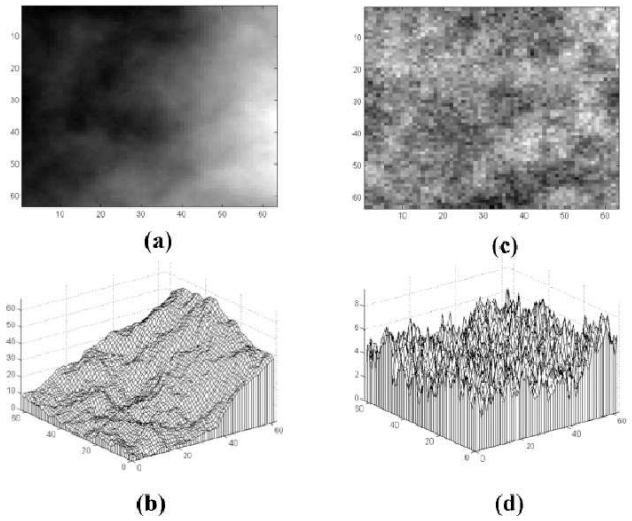

Fig. 4. (a) Synthetic fractal texture with fractal dimension $D = 2.20$, (b) 3-D representation of this texture, (c) Synthetic fractal texture with fractal dimension $D = 2.80$, (d) 3-D representation of this texture.

TABLE I
FRACTAL DIMENSION FOR SYNTHETIC SURFACES (IMAGES 63-BY-63)

Original dimension	Estimated dimension mean±standard deviation
2.05	2.103 ± 0.102
2.10	2.197 ± 0.138
2.20	2.276 ± 0.139
2.30	2.311 ± 0.124
2.40	2.451 ± 0.116
2.50	2.521 ± 0.124
2.60	2.587 ± 0.117
2.70	2.721 ± 0.096
2.80	2.820 ± 0.062
2.90	2.907 ± 0.042
2.95	2.958 ± 0.018

TABLE II
FRACTAL DIMENSION FOR SYNTHETIC SURFACES CALCULATED IN IRREGULAR REGIONS OF INTEREST

Original dimension	Estimated dimension irregular regions mean±standard deviation
2.05	2.122 ± 0.113
2.10	2.141 ± 0.109
2.20	2.248 ± 0.132
2.30	2.314 ± 0.137
2.40	2.467 ± 0.107
2.50	2.560 ± 0.116
2.60	2.610 ± 0.118
2.70	2.704 ± 0.143
2.80	2.821 ± 0.061
2.90	2.903 ± 0.075
2.95	2.964 ± 0.015

B. Pantomogram (panoramic radiograph)

Pantomogram is a panoramic radiographic record obtained by a pantomograph. It shows maxillary and mandibular dental arches and their associate structures. Pantomograms were digitized with an Umax Alpha Vista II scanner (LaserSoft Imaging Inc., USA), interfaced through a scan software program (SilverFast Applications) to a computer. Fig. 5 shows the pantomogram with two marked regions: normal region A, and region B with pathological changes.

In the process of reinclusion, the erupting or already erupted tooth submerges in the bone creating a variety of clinical problems. The diagnosis of reinclusion is based mainly on recognized clinical and radiological symptoms. The characteristics of reincluded teeth in pantomograms include pathological root resorption and changes to the adjacent bone structures. Quantitative evaluation of bone changes may be estimated by means of fractal dimension.

The sizes and shapes of the ROI-s were determined by the sizes and shapes of the interdental bone to be analyzed. If the number of elements in the analyzed region of a picture is too small the differentiation between various pathological states may fail.

Figure 6 shows the regular regions of interest from Fig. 5. Inside of these regions irregular ROI-s are marked. The

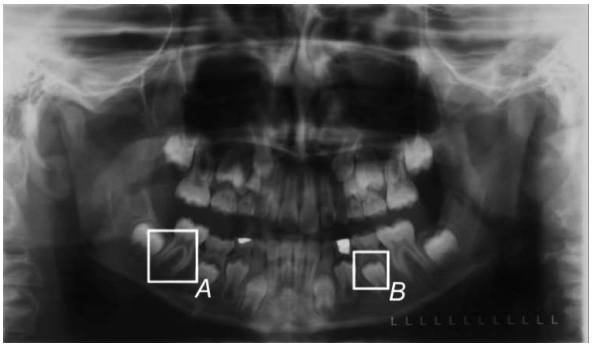

Fig. 5. Panoramic radiograph with marked regions: normal region A, and region B with pathological changes.

TABLE III
RESULTS OF FRACTAL ANALYSIS IN IRREGULAR AND REGULAR REGIONS OF INTEREST MARKED IN FIG. 6

Regions	Fractal dimension	Number of scales
Regular ROI – Fig. 6(a)	2.657	20096
Regular ROI – Fig. 6(b)	2.865	10584
Irregular ROI – Fig. 6(a)	2.513	2305
Irregular ROI – Fig. 6(b)	2.245	1352

sizes in pixels of regular ROI-s are: 245×245 (Fig. 6(a) and 175×175 (Fig. 6(b)). Table III summarizes the results of fractal analysis in all regular and irregular regions. When the irregular ROI contain the boundary and fragment of the teeth the value of fractal dimension is low ($D = 2.245$).

C. Nuclear medicine scan — scintigram

Scintigraphy is a method of organ visualizing which enables us to describe its shape, dimensions and position by means of the radiopharmaceutical tracers accumulated in the organ after oral or intravenous administration to the patient [31]. Nuclear medicine scans (scintigrams), which are pictures obtained by gamma camera have small image matrices (128×128 or 64×64). Fig. 7 illustrates the result of fractal analysis of liver scan in the irregular regions of interest. The region with fractal dimension $D = 2.53$ corresponds to the foci of metastases. Low value of fractal dimension $D = 2.16$ is in the region containing the boundary of the liver. In the region within of the liver $D = 2.68$.

V. CONCLUDING REMARK

As it is difficult to fit the entire regular region of interest within the examined organ with simultaneous inclusion of the relevant fragment avoiding the influence of boundaries and other kinds of unnecessary structures at the same time, we introduced a method to calculate the fractal dimension I irregular ROI-s. The results obtained show that our findings may be of great importance for diagnostic purposes.

REFERENCES

[1] T. Nonnemacher, G.A. Losa, and E.R. Weibel, Eds. *Fractals in biology and medicine*, Basel: Birkhäuser Verlag, 1994.
[2] T. R. Nelson, "Fractals. Physiologic complexity, scaling and opportunities for imaging", *Invest. Radiol.*, vol. 25, pp 1140-1148, 1990.

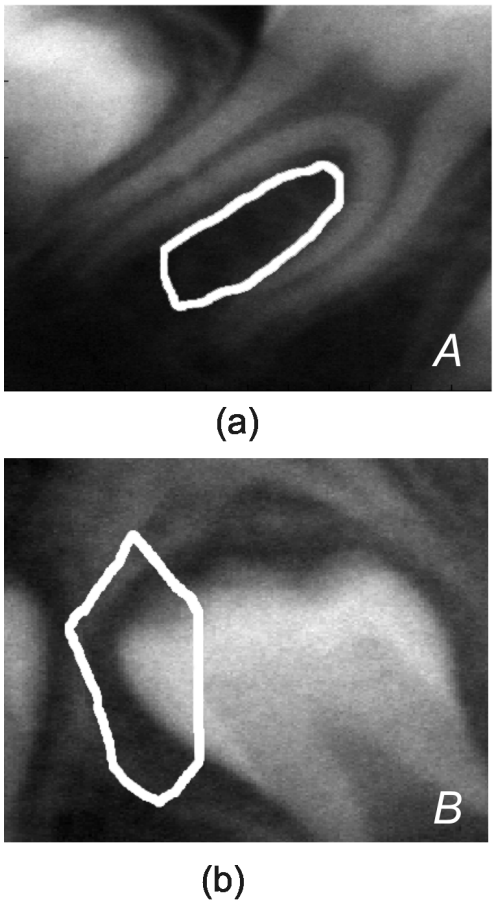

Fig. 6. The regions A and B from Fig. 5.

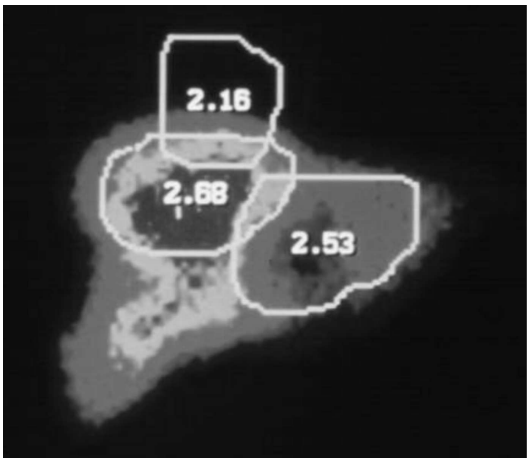

Fig. 7. Fractal analysis of liver scan (image 128×128) in the irregular regions of interest. The region with fractal dimension $D = 2.53$ corresponds to the foci of metastases. Low value of fractal dimension $D = 2.16$ is in the region containing the boundary of the liver.

[3] B. B. Mandelbrot and J. W. Van Ness, "Fractional Brownian motions, fractional noises and applications", *SIAM Rev. Soc. Ind. Appl. Math.*, vol. 10(4), pp 422-437, 1968.

[4] F. Hausdorff, "Dimension und äußeres Maß", *Math. Ann.*, vol. 79, pp 157-179, 1918.

[5] A. Besicovitch, "On the fundamental properties of linearly measurable plane sets of points", *Math. Ann.*, vol. 98, pp 422-464, 1928.

[6] C. B. Caldwell, E. L. Moran, and E. R. Bogoch, "Fractal dimension as a measure of altered trabecular bone in experimental inflamatory arthritis", *J. Bone Miner. Res.*, vol. 13(6), pp 978-985, 1998.

[7] K. C. Clarke, "Computation of the fractal dimension of topographic surfaces using the triangular prism surface area method", *Comp. Geosci.*, vol. 12, pp 713-722, 1986.

[8] T. J. Dennis and N. G. Dessipris, "Fractal modelling in image texture analysis", *Radar and Signal Process., IEE Proc. F*, vol. 136, pp. 227-235, 1989.

[9] B. J. Super and A. C. Bovik, "Localized measurement of image fractal dimension using Gabor filters", *J. Visual Commun. Image Represent.*, vol. 2, pp 114-128, 1991.

[10] P. Maragos and F. K. Sun, "Measuring the fractal dimension of signals: morphological covers and iterative optimization", *IEEE Trans. Signal Process.*, vol. 41(1), pp 108-121, 1993.

[11] S. Peleg, J. Naor, R. Hartley, and D. Avnir, "Multiple resolution texture analysis and classification", *IEEE Trans. Pattern Anal. Mach. Intell.*, vol. 6(4), pp 518-523, 1984.

[12] J. B. Bassingthwaighte, "Physiological heterogeneity, fractals link determinism and randomness in structures and functions", *News Physiol. Sci.*, vol. 3, pp 5-10, 1988.

[13] E. Oczeretko, F. Rogowski, and D. Jurgilewicz, "Fractal analysis of nuclear medicine scans", in *Fractals in Biology and Medicine*, G. A. Losa, D. Merlini, E. R.Weibel, and T. Nonnemacher, Eds. Vol. II, Basel: Birkhäuser Verlag, pp 326-334, 1998.

[14] F. Bianchi and R. Bonetto, "FERImage: an interactive program for fractal dimension, d(per) and d(min) calculations", *Scanning*, vol. 23(3), pp 193-197, 2001.

[15] C. C. Chen, J. S. Daponte, and M. D. Fox, "Fractal feature analysis and classification in medical imaging", *IEEE Trans. Med. Imaging*, vol. 8, pp 133-142, 1989.

[16] R. Voss, "Random Fractals: Characterization and measurement", in *"Scaling Phenomena in Disordered Systems"*, R. Pynn and A. Skjeltorp, Eds. New York: Plenum, pp 1-11, 1986.

[17] S. S. Chen, J. M.Keller, and R. M. Crownover, "On the calculations of fractal features from images", *IEEE Trans. Pattern Anal. Mach. Intell.*, vol. 15(10), pp 1087-1090, 1993.

[18] G. A. Losa, D. Merlini, T. Nonnemacher, and E. R. Weibel, Eds. *Fractals in Biology and Medicine Volume*, Vol. II, Basel: Birkhäuser Verlag, 1998.

[19] G. A. Losa, D. Merlini, T. Nonnemacher, and E. R. Weibel, Eds. *Fractals in Biology and Medicine*, Vol. III, Basel: Birkhäuser Verlag, 2002.

[20] G. A. Losa, D. Merlini, T. Nonnemacher, and E. R. Weibel, Eds. *Fractals in Biology and Medicine*, Vol. IV, Basel: Birkhäuser Verlag, 2005.

[21] D. Chappard, P. Guggenbuhl, E. Legrand, M. F. Basle, and M. Audran, "Texture analysis of X-ray radiographs is correlated with bone histomorphometry", *J. Bone Miner. Metab.*, vol. 23, pp 24-29, 2005.

[22] K. M. Iftekharuddin, W. Jia, and R. Marsh, "A fractal analysis of tumor in brain MR images", *Mach. Vision and Appl.*, vol. 13, pp 352-362, 2003.

[23] T. Mustonen, T. Koivisto, E. Vanninen, R. Vanninen, and J. Kuikka, "Cerebral perfusion heterogeneity and complexity in patient in acute subarachnoid haemorrhage", *Nucl. Med. Commun.*, vol. 27(2), pp 157-164, 2006.

[24] J. Gärding, "Properties of fractal intensity surfaces", *Pattern. Recog. Lett.*, vol. 8, pp 319-324, 1988.

[25] J. T. M. Verhoeven, "Improvment of echographic image quality by data analysis and processing", *Ultrasound Imaging*, vol. 15, pp 304-323, 1993.

[26] E-L. Chen, P.-C. Chung, C.-L. Chen, H.-M. Sai, and C.-I. Chang, "An automatic diagnostic system for CT liver image classification", *IEEE Trans. Biomed. Eng.*, vol. 45(6), pp 783-794, 1998.

[27] C. M. Wu, Y. C. Chen, and K. S. Hsieh, "Texture features for classification of ultrasonic liver images", *IEEE Trans. Med. Imaging*, vol. 11(2), pp 141-152, 1992.

[28] L.M. Kaplan and C.C.J. Kuo, ”An improved method for 2-D self similar image synthesis”, *IEEE Trans. Image Process.*, vol. 5(5), pp 751-760, 1995.
[29] G.J. Battaglia, ”Mean square error”, *AMP J. Tech.*, vol. 5, pp 31-36, 1996.
[30] A. Eke, P. Herman, J. B. Bassingthwaighte, G. M. Raymond, and D. B. Percival, ”Physiological time series: distinguish fractal noises from motion”, *Pflügers Arch.-Eur. J. Physiol.*, vol. 439, pp 403-415, 2000.
[31] C.G. Eckel, A.G. Williams, and F.A. Metler, ”Introducing to signal processing in nuclear medicine”, in *Practical computer applications in radionuclide imaging*, A.G. Williams and C.G. Eckel, Eds. Churchill Livingstone, pp 1-31, 1987.